Energy Technology
Generation, Conversion, Storage, Distribution
www.entechnol.de

Pencil Scripted Ultrathin Graphene Nanostructure as Binder-Free Battery-Type Electrode for Li-Ion Micro-Capacitors with Excellent Performance

*Kondachan Parambil Shadiya, Madhusoodhanan Lathika Divya, Yun-Sung Lee, and Vanchiappan Aravindan**

Herein, a binder-free graphene nanostructure anode formulated by drawing on Cu current collector with a commercial 10B pencil is reported. The prepared pencil-trace electrode (10B pencil graphite, 10B PG) shows an excellent cycling profile with ≈87% capacity retention characteristics after 1000 cycles. Further, a dual-carbon lithium-ion capacitor (LIC) is fabricated using the pencil-trace electrode as battery-type electrode and commercial activated carbon (AC) as capacitor electrode in aprotic organic solutions. The 10B PG is pre-lithiated prior to LIC fabrication to ensure an ample supply of Li-ions during cycling. The developed LIC, 10B PG/AC assembly, displays a remarkable energy density of 109.9 Wh kg^{-1} irrespective of the applied current density, that is, power.

1. Introduction

Alternative energy sources, for instance, renewable energy resources and new environmentally sustainable energy-storage systems, have to be developed to combat the energy crisis and environmental issues. However, renewable energies are intermittent, whereas energy-storage systems ensure continuous energy delivery.[1] The two core technologies that are used to store electrochemical energy are rechargeable batteries and supercapacitors. Among the secondary batteries, lithium-ion batteries (LIBs) have gained owing to the high specific energy, low self-discharge rate, and shape versatility.[2] However, it exhibited limited power capabilities and cycle life.[3] The reversible insertion of Li-ions between anode and cathode through the electrolyte is the basic principle for LIBs. The LIBs are the unanimous choice for portable electronics and are growing in demand for electric vehicles (EV) and aerospace applications.[4] The supercapacitors group includes electric double-layer capacitors (EDLCs), in which the physisorption of ions (cations and anions) at the electrode surface is the mechanism of energy storage. EDLCs have elevated specific power, fast charge–discharge capability, and long service life but restricted charge-storage capacity.[5] The self-discharge is one more major problem with all the EDLCs.[6]

Merging a battery and EDLC-type electrodes in the same device is anticipated to display combined features of both LIB and EDLC. Hence, the lithium-ion capacitor (LIC) concept has been developed as a promising next-generation energy-storage device.[7–15] In LIC, the LIB electrode, that is, battery-type electrode, is used as a negative electrode to obtain high energy, and the EDLC electrode is employed as a counter electrode to achieve high power capability.[16–18] The LIC was first conceptualized by Amatucci et al.[19] Various applications of LICs are already demonstrated, like auxiliary energy storage for intermittent photovoltaic and wind power sources, power backup in servers and storage devices, power sources for small appliances, and automobiles during deaccelerating and stopping.[20]

To obtain high energy density, the LICs should be fabricated with carbonaceous material as the battery-type electrode, and activated carbon (AC) as a capacitive electrode is regarded as the best choice among many available combinations between the LIB and EDLC electrodes. The reason is the lower Li-insertion/extraction potential of the carbonaceous materials, especially graphitic carbon, and the excellent stability of AC at the wide potential range.[21] The pre-lithiation process is desperately required to operate in such dual-carbon-based LICs. This compensates for the potential loss of active lithium so as to obtain higher gravimetric energies.[22] It is achieved by storing a certain amount of active lithium in the anode, that is, LiC_6 prior to the fabrication of the LICs. The efficiency of the anode electrode largely contributes to the Li-storage capacity, that is, energy density. Graphite has been widely used as anode material for LIBs because of its lower redox potential (< 0.1 V vs Li), decent capacity (≈372 mAh g^{-1}), low cost, abundant resources, and excellent stability. Graphite can be easily exfoliated by mild external force and eventually deposited onto the rough surface due to its layered structure. The Li-storage capacity of the LIC anode can be enhanced by replacing traditional graphite with pencil lead. The pencil is mainly composed of graphite with partially intercalated clay particles and wax. The clay is

K. P. Shadiya, M. L. Divya, V. Aravindan
Department of Chemistry
Indian Institute of Science Education and Research (IISER)
Tirupati 517507, India
E-mail: aravindan@iisertirupati.ac.in

Y.-S. Lee
School of Chemical Engineering
Chonnam National University
Gwang-ju 61186, Republic of Korea

The ORCID identification number(s) for the author(s) of this article can be found under https://doi.org/10.1002/ente.202200205.

DOI: 10.1002/ente.202200205

predominantly composed of SiO_2 and a minor amount of other metal oxides. Generally, the pencils are divided into grades, such as H, B, and HB, and they depend on the graphite to clay ratio. H stands for "hard," B stands for "black" (these pencils are considered soft), and HB stands for hard black, which means medium–hard. These notations are usually preceded by numbers. The higher number indicates, the harder or softer the pencil is. Hardness is mainly determined by the presence of higher clay content, while blackness originated from higher graphitic carbon concentration. Black deposits, which contain graphitic carbon material, are produced when drawn with a pencil on a rough surface. The multilayers of graphene contained in the deposit can facilitate conductive pathways for Li-ion movement despite the presence of resistive clay.[23]

Polymeric binders are normally used in electrodes to ensure good adhesion of active material and conductive agent on the current collector. However, the use of binder can cause thermal runaway, limited rate capability, and reduced lifetime due to inevitable side reactions between the binder and electrolyte.[24] The binder-free electrodes show better capacity, cycling profile, and rate performance than the conventional formulation of the polyvinylidene fluoride (PVdF), active material, and carbon black system with *N*-methyl-2-pyrrolidone (NMP) solvent as these composite electrodes exhibit a high Li-ion and electronic conductivity, notable electrolyte wettability, strong bonding strength, and large volume expansion space.[25] In addition, the toxicity and the expensive nature of NMP (14.5% of overall LIB cost) cause the necessity of a solvent recovery system.[26] Electrode fabrication without slurry coating can lower the overall cost of the LIB/LIC system and also offer active charge transfer due to direct conductive pathways within the electrode.[23] Here, we introduce a binder- and solvent-free pencil-trace electrode formed by simple drawing of a regular 10B grade graphite drawing pencil on Cu current collector, and the performance of such electrode is studied in half-cell assembly. Further, we also assembled a dual-carbon Li-ion micro-capacitor with a pre-lithiated form of such pencil-trace electrode as anode and AC cathode.

2. Results and Discussions

2.1. Physical Properties

Powder X-Ray diffraction (XRD) was conducted to investigate the crystal structure and the phase composition of 10B PG, which is scribbled on Cu substrate **Figure 1**a. The figure shows that the XRD pattern of 10B PG shows a prominent and characteristic peak at around 26.67°, corresponding to the (002) crystallographic planes of graphite with an interplanar spacing of 3.34 Å. A less intense peak observed at 54.6° corresponds to the (004) planes with a *d* spacing of 1.9 Å. The same characteristic peak was observed for the case where 10B PG was scribbled on Cu foil by eliminating the peaks of Cu. The peaks positioned at 26.6° also correspond to the (101) planes of the hexagonal crystal structure of SiO_2 that matches with the standard reference, which indicates the presence of silicon in the pencil graphite sample in the form of clay. The quality of graphite in PG material was analyzed by Raman spectroscopy. Figure S1, Supporting Information, shows mainly G band 2G band corresponding graphitic form of carbon. The less intense D band (defect band) with an intensity ratio (I_D/I_G) value of 0.16 indicates the high crystallinity of PG material. TGA analysis Figure 1b, a four-step

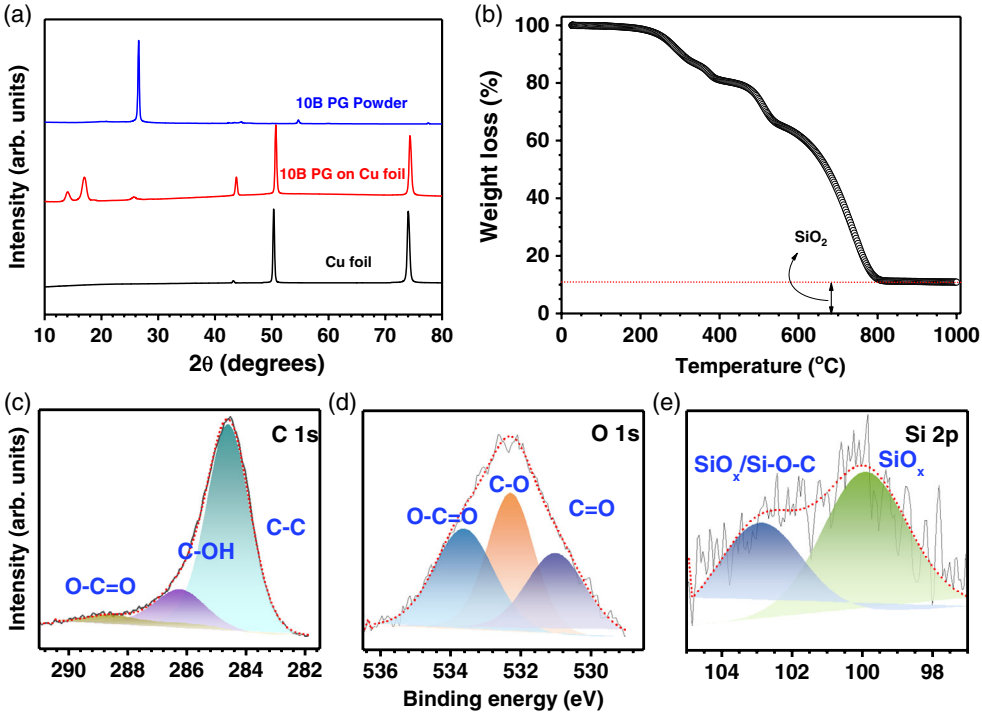

Figure 1. Physical characterization of 10B PG: a) X-Ray diffraction (XRD), b) Thermal gravimetric analysis (TGA) curve, and c) deconvoluted X-ray photoelectron spectroscopy (XPS) spectra of C 1s, d) O 1s, and e) Si 2*p*.

decomposition pattern, showed 89.1 wt% loss in sample weight as the temperature was beyond 800 °C, and it belongs to the clay component, SiO_2 (≈11 wt%). The weight loss is stabilized at 800 °C, indicating the removal of all the carbonaceous traces in the sample. This implies a higher carbon to clay ratio in the 10B PG because all the carbon content would get decomposed below 1000 °C. Oxidation of carbon can be seen beyond 400 °C, in which ≈50% of the sample got decomposed at ≈673 °C. The higher decomposition temperature infers a high degree of crystallization of the graphitic carbon.

The X-Ray photoelectron spectroscopy (XPS) studies were performed to get information about the surface elemental chemical composition and the binding energy of the pencil graphite surface. Three prominent XPS bands have appeared at 284.6 (C 1*s*), 532 (1*s*), and 99.5 eV (Si 1*s*) in the survey scan spectrum. The C1*s* spectra can be decomposed into three components: 284.6, 286.22, and 288.63 eV, which correspond to primary C–C/C–H, C–O, and COO- groups, respectively,[27] as shown in Figure 1c. This clearly indicates that the 10B PG sample contains a significant amount of sp^2 carbon. The deconvoluted O 1*s* spectra showed Lorentzian peaks at 532.28, 533.6, and 531 eV, which are associated with C–O, COO-, and C = O functionalities, respectively,[28,29] as shown in Figure 1d. Deconvolution of Si 2*p* spectra shows two main components at 99.92 and 102.87 eV corresponding to SiO_x and SiO_x/Si–O–C, respectively,[30] as shown in Figure 1e. Scanning electron microscopy (SEM)-energy dispersive spectroscopy (EDS) analysis and elemental mapping of the elements C, O, and Si were performed to determine the distribution of these elements in pencil graphite.

The surface morphological features of the pencil-trace powder sample were analyzed using field-emission SEM (FE-SEM) at different magnifications, which showed the flaky structures of varying sizes with agglomeration, **Figure 2**a–c and S2, Supporting Information. These microstructure images captured by FE-SEM showed similar morphology as that of graphite. Generally, the flaky kind of morphology is considered to have a high degree of crystallinity. The cross-sectional image of 10B PG scribbled on Cu substrate was taken to differentiate it from the Cu surface, and the coating thickness was estimated to be ≈1.7 µm, Figure 2d. Transmission electron microscope (TEM) image of the 10B PG sample is shown in Figure 2e. The presence of the layered structure of pencil graphite can be confirmed from high-resolution TEM (HR-TEM) images of 10B PG, Figure 2f. The interlayer spacing between graphene layers was measured as 0.326 nm. Selected area electron diffraction (SAED) in TEM was used to analyze the crystalline nature of the 10B PG sample, which showed hexagonal patterns with bright spots, Figure 2g. Elemental mapping studies, Figure 2h–k, showed that carbon is densely distributed throughout the mapping area. The distribution of oxygen moieties is denser compared to silicon in the sample.

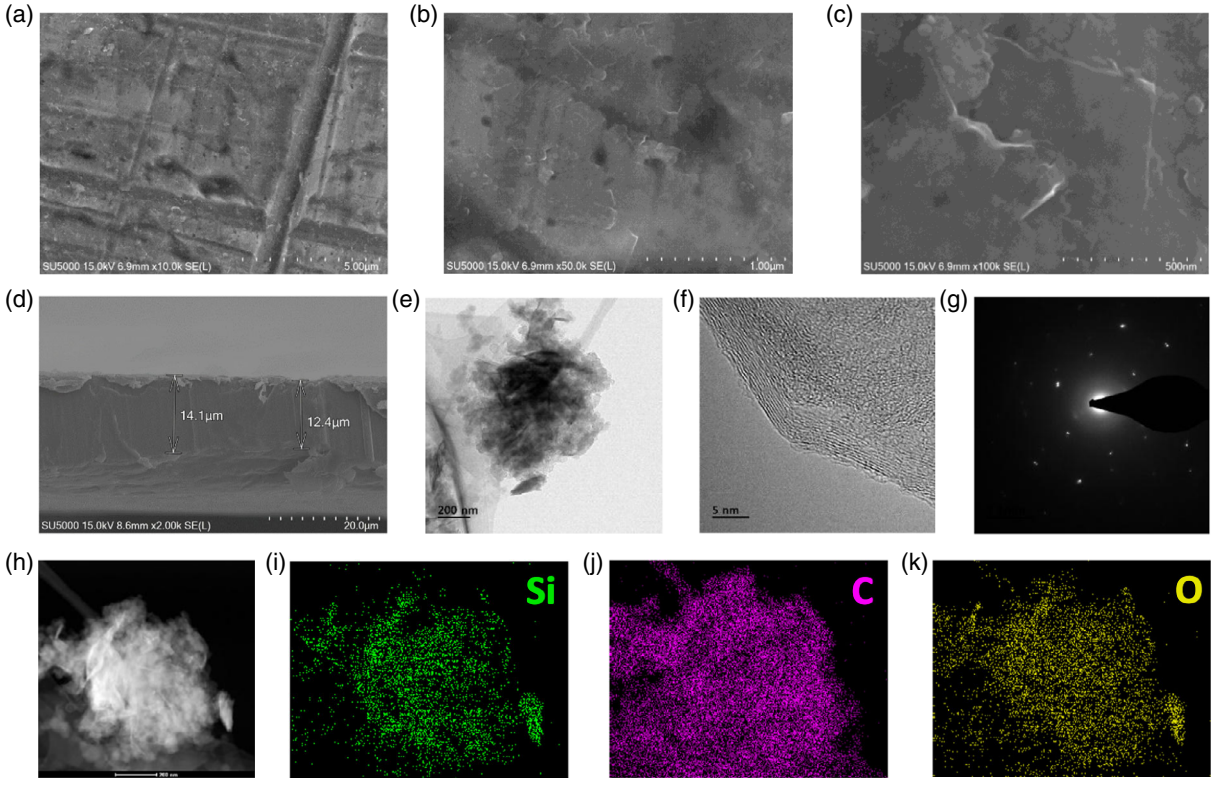

Figure 2. a–c) Field-emission scanning electron microscope (FE-SEM) images of 10B PG with different magnifications, d) SEM cross-section image of 10B PG, e) transmission electron microscope (TEM) image of 10B PG, f) high-resolution TEM (HR-TEM) image of 10B PG with lattice fringes, g) selected area electron diffraction (SAED) pattern of 10B PG, and h–k) elemental mapping images of 10B PG sample.

2.2. Electrochemical Properties

Figure 3a,b shows the cyclic voltammetry (CV) traces of half-cells of electrodes made by scribbling Cu-foil with 10B PG pencil and coated 10B PG powder on Cu foil, respectively, tested between 2.5 and 0.005 V versus Li at various scan rates. The small and multiple peaks observed below 0.2 V versus Li indicate the Li-insertion into graphene layers via the staging process. Figure S3, Supporting Information illustrates the typical CV profile of 10B PG scribbled electrode at a scan rate of 0.1 mV s^{-1}. As the plot of peak current, i_p (mA) versus square root of the scan rate, ($V^{1/2}$ $s^{-1/2}$) is linear (Figure 3c), the electron transfer process is electrochemically reversible where Li-ions are freely diffusing as described by the Randles–Sevcik equation.[31] For the scribbled case, the prominent peaks were positioned at 0.19, 0.09, and 0.06 V versus Li^+/Li for the reduction upon cathodic scans, and peaks positions around 0.23, 0.14, and 0.10 V versus Li^+/Li for oxidation process during the anodic scans, respectively. These peaks correspond to characteristic Li_xC phase transformations that are observed during Li-insertion/extraction processes, as reported in the literature.[32,33] The cathodic/anodic peaks in the subsequent cycles of the same scan rate are overlapping, demonstrating the high reversibility of the Li-insertion/extraction into/from the pencil trace.[34] For faster scan rates, higher currents are observed as a result of a decrease in the size of the diffusion layer.[31] Accordingly, the diffusion coefficient of Li-ions in scribbled pencil electrode was calculated as 7.86×10^{-11} cm^2 s^{-1} from anodic peak current and 2.56×10^{-10} cm^2 s^{-1} from cathodic peak current. For the case of 10B PG cast by the conventional process, the corresponding diffusion coefficients are 3.44×10^{-9} and 1.15×10^{-8} cm^2 s^{-1}, which are in good agreement with the values reported in the literature and slightly higher diffusivity than pencil scribbled one.[35,36] Binder-free electrodes generally exhibit high Li^+ conductivity[25]; the lower value of diffusion in this study may be due to less active material loading.[37] Also, there is a possibility of a non-Faradaic Li-adsorption/desorption process rather than the perfect Li-insertion process owing to the thin layer of pencil trace/coating, which has a lot of disorders/exfoliation in the carbonaceous material. More

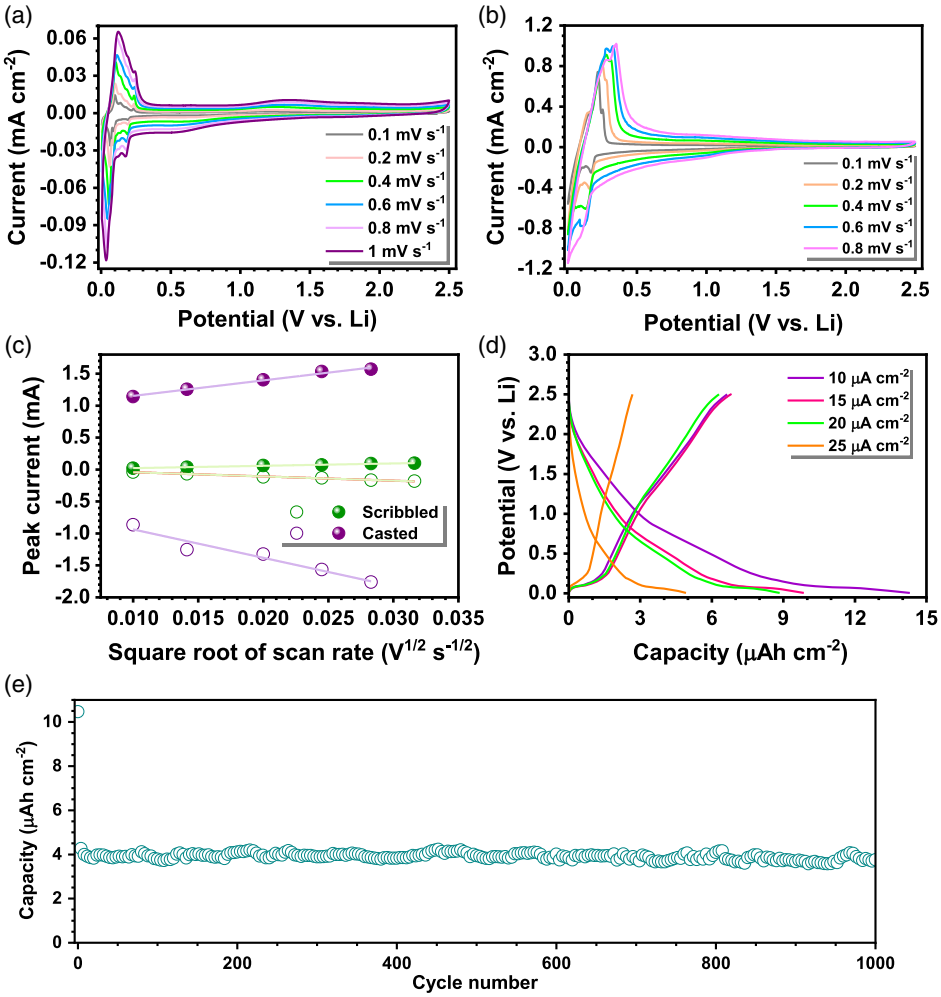

Figure 3. Typical cyclic voltammetry (CV) of 10B PG electrode made by a) scribbling on Cu substrate, b) casting on Cu substrate, and c) plot of peak current, i_p (mA) versus square root of the scan rate ($V^{1/2}$ $s^{-1/2}$), Half-cell performance of Li/10B PG cell: d) galvanostatic charge–discharge profile of 10B PG at current densities 10,15, 20, and 25 μA cm^{-2}, and e) plot of discharge capacity versus cycle number at 30 μA cm^{-2}.

specifically, in pencil-trace electrode, in addition to the faradaic Li-intercalation process, non-Faradaic capacitive storage is also dominant, which is eventually reflected in the Li-diffusivity. Nevertheless, in coated/bulk electrodes, the Li-intercalation reaction is dominant. The nature of galvanostatic curves will provide the more clear picture on this aspect.

Figure 3d displays the typical charge–discharge curves of the pencil-trace electrode at different current densities (10, 15, 20, and 25 μA cm^{-2}) tested between voltage range 0.005–2.5 V versus Li. A drop in capacity is observed on swapping from a lower to a higher current rate due to the concentration polarization of Li-ions in the electrode resulting from a diffusion-limited process.[23] The discharge curve was tested with a current density of 10 μA cm^{-2} display plateaus in the voltage range between 0.81 and 0.72 V versus Li and between 0.1 and 0.005 V versus Li, which corresponds to Li-ion intercalation into graphite. The scribbled electrode delivered a discharge capacity of 33.37 μAh cm^{-2} in the first cycle and a corresponding charge capacity of 6.84 μAh cm^{-2}. The initial Coulombic efficiency was as low as 20.5% due to the formation of solid electrolyte interface (SEI) film.[23] The half-cell delivered a capacity of 14.3 and 6.64 μAh cm^{-2} for the successive discharge and charge, respectively, corresponding to an increased Coulombic efficiency of 46.43%. The long-term cycling profile of the pencil trace at a current density of 30 μA cm^{-2} is presented in Figure 3e. The charge–discharge profiles in all the cycles show a similar shape, indicating that the electrochemical profile is stable. The cell renders the capacity retention of ≈87% after the 1000th cycle (excluding first discharge), meaning an excellent cycling performance for the pencil-trace electrode. In contrast, perfect plateau is observed for the case of coated/bulk electrode, which confirms the Faradaic process is predominant (Figure S4, Supporting Information). However, in the case of scribbled electrode, the absence of perfect plateaus indicate the presence both Faradaic (redox reaction) and non-Faradaic (physisorption) process.

The charge–discharge profile of commercial AC is linear, which shows the non-Faradaic process of adsorption and desorption. The half-cell displayed an initial discharge capacity of 676 μAh cm^{-2}. To examine the cycling stability, the AC electrode was galvanostatically charged and discharged at a current density of 1000 μA cm^{-2} between 1.5 and 4.5 V versus Li for 350 cycles. The half-cell showed Coulombic efficiency of >99% after the 350th cycle, which indicates excellent electrochemical reversibility of AC via the non-Faradaic process, Figure S5, Supporting Information.

2.3. Li-Ion Capacitor: 10B PG versus AC

Before the fabrication of LIC, pre-lithiation of the pencil-trace electrode was achieved by two complete galvanostatic discharge–charge cycles followed by a deep discharge with the Li metal at a current rate of 10 μA cm^{-2} between 0.005–2.5 V versus Li. During the lithiation process, it is observed that the Li/10B PG potential difference decreased with time, from an initial value of ≈2.7 to <100 mV versus Li, indicating the storage of Li-ions into the carbonaceous nanostructures toward the formation of the binary graphite intercalation compound (GIC).[38] After making sure that the open circuit potential (OCP) of the Li pre-doped half-cell is below 100 mV, it was immediately taken for cell fabrication by combining with an AC electrode in the glove box.

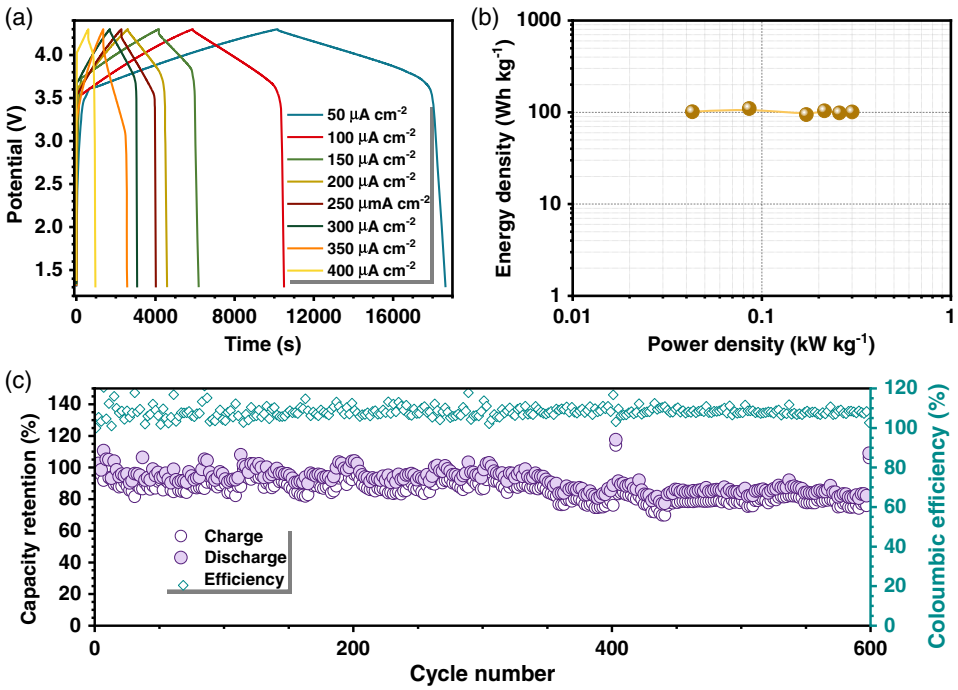

Figure 4. Electrochemical performance of the fabricated lithium-ion capacitor (LIC) a) voltage versus time profile for varying current rates, b) Ragone plot, and c) cycling performance at a current rate of 100 μA cm^{-2}.

An LIC cell was assembled with the pre-lithiated carbonaceous electrode, LiC_6 as a battery-type electrode, and AC as the counter electrode. The open-circuit voltage of around 2.7 V was displayed by the fabricated LIC. The LIC was charged/discharged between 1.3 and 4.3 V at various current rates 50, 100, 150, 200, 250, 300, 350, and 400 μA cm^{-2} (**Figure 4**a). The charge–discharge curve of the fabricated LIC was dissimilar to that of either PG or AC, which indicates the involvement of two different charge-storage mechanisms, that is, adsorption/desorption and intercalation/deintercalation. As the current rate was increased, a reduction in discharge time was observed. The Ragone plot of the fabricated LIC is shown in Figure 4b. For energy density calculation, the specific capacity value was multiplied by the working potential. Power density values were obtained by dividing energy density values by the discharge time. (Energy density and power density calculation is based on the active material weight of AC (≈8 mg) alone as the mass of PG is negligible.). Accordingly, the LIC delivered a maximum gravimetric energy density of 109.9 Wh kg^{-1} at a power density of 0.086 kW kg^{-1}. Absolutely there is no reduction in the energy density (100.7 Wh kg^{-1}), even at the power density of 0.301 kW kg^{-1}. This is an ideal case and is desperate for any LIC perspective as a battery-type electrode. This is certainly possible with the fabrication of the electrode without any binder or conductive additives. Further studies are in progress with the optimization of the mass loadings and fabrication of symmetric electrodes to realize the charge-storage capability. Also, importance will be given to improving the cycling profile of the LIC as well. The cyclability of the LIC was tested for 1000 cycles at a current rate of 100 μA cm^{-2} and is presented in Figure 4c. At the end of 600 cycles, the LIC could retain ≈82% of its initial capacity value.

3. Conclusion

In summary, we presented the assembly of LIC having binder-free pencil-trace electrodes 10B PG as anode and AC cathode. PG anode was prepared by a simple process of scribbling 10B pencils on Cu foil. We could observe that PG material with intercalated clay showed better rate capability and cyclic stability as the clay could act as a structural buffer and provide high electrical conductivity. In addition, nano range electrode material could avoid aggregation of electrode material and alleviate volume expansion issues during cycling. The binder-free PG-trace electrode-based LIC unveiled a higher energy density than conventional supercapacitors. By mass-balancing of positive and negative electrodes, better performance of such LICs, which are highly useful for practical applications, can be accomplished by further research.

4. Experimental Section

Physical Characterization: Powder XRD analysis (ULTIMA-IV, Rigaku, ARBL-RAD) was explored with monochromatic Cu Kα radiation ($\lambda = 0.15406$ nm) at a scanning rate of 0.5° min^{-1} to examine the crystal structure of 10B PG. XPS (Multilab 2000, UK) was carried out to characterize the surface chemical composition of the 10B PG sample. Surface morphological features and internal structure of 10B PG were studied using FE-SEM (S 4700, Hitachi, Japan) and HR-TEM (JEM-2000, EX-II, JEOL, Japan), respectively. Thermal gravimetric analysis (TGA, Shimadzu, Japan TG-50) was performed to confirm the ratio of graphite to clay in the sample.

Cell Construction and Electrochemical Studies: The 10B grade pencil (Kasimir Aavjo, China) was procured from the market to prepare the pencil-trace electrode. The current collectors used for the cell fabrication were commercially available Cu foil and stainless steel, SS (Goodfellow, UK) mesh. The electrode was formulated by drawing with a 10B grade pencil on Cu-foil by hand, and a circle of 14 mm diameter was punched from it by using an electrode cutter. It was then dried under a vacuum at 75 °C for 4 h.

The average mass and the thickness of scribbled active material were estimated as ≈14 μg cm^{-2} and 1.7 μm in the pencil-trace electrode, respectively. The commercial AC (Kuraray, Japan) electrode was prepared by combining AC (YP 80F, surface area: 2100 m^2 g^{-1}, pore volume: 0.97 mL g^{-1}), acetylene black, teflonized acetylene black (TAB-2) binder at a weight ratio of 8:1:1 by using a mortar and pestle with ethanol. The mixture was pressed onto a 14 mm diameter SS mesh that served as a current collector and dried under vacuum at 75 °C for 4 h.

To evaluate the electrochemical storage performance of the binder-free pencil-trace electrodes, the CR-2016 coin cells were fabricated in an Ar-filled glove box (H_2O and $O_2 < 0.1$ ppm) with lithium metal as the counter/reference electrode and Whatman paper (1825-047, GF/F) as a separator. The 1.0 M $LiPF_6$ dissolved in a mixture of ethylene carbonate (EC) and dimethyl carbonate (DMC) (1: 1 by volume) from Tomiyama, Japan; electrolyte was employed as the electrolyte solution. The electrochemical performance of pencil-trace electrodes without any binder and AC electrodes with a binder in the standard coin-cell assembly were examined by galvanostatic charge–discharge (GCD) cycling and characterized in a Battery cycling system, BCS 805 (Biologic, France). The pencil-trace electrode was tested at various current rates like 10, 15, 20, and 25 μA cm^{-2} in the voltage range of 0.005–2.5 V versus Li at room temperature. The CV studies were conducted in the potential range of 0.005–2.5 V versus Li at various scan rates. Similarly, the Li/AC cell was galvanostatically cycled at a current rate of ≈1000 μA cm^{-2} for 350 cycles in the voltage range 1.5–4.5 V versus Li.

Supporting Information

Supporting Information is available from the Wiley Online Library or from the author.

Acknowledgements

M.L.D. wishes to thank the funding through Women Scientist Scheme-B (DST/WOS-B/2018/2039) from the KIRAN division of the Department of Science & Technology (DST), Government of India. Y.S.L. acknowledges the financial support from the National Research Foundation of Korea (NRF) grant funded by the Korean government (Ministry of Science, ICT & Future Planning) (Grant no. 2019R1A2C1007620). V.A. acknowledges financial support from the DST for Swarnajayanti Fellowship (DST/SJF/PSA-02/2019-20).

Conflict of Interest

The authors declare no conflict of interest.

Data Availability Statement

The data that support the findings of this study are available from the corresponding author upon reasonable request.

Keywords

binder-free electrodes, graphite anodes, lithium-ion capacitors, pencil-trace electrodes

Received: March 2, 2022
Revised: April 22, 2022
Published online: May 4, 2022

[1] E. Drury, P. Denholm, R. Sioshansi, *Energy* **2011**, *36*, 4959.
[2] D. P. Dubal, O. Ayyad, V. Ruiz, P. Gómez-Romero, *Chem. Soc. Rev.* **2015**, *44*, 1777.
[3] M. Soltani, S. H. Beheshti, *J. Energy Storage* **2021**, *34*, 102019.
[4] J. Ajuria, E. Redondo, M. Arnaiz, R. Mysyk, T. Rojo, E. Goikolea, *J. Power Sources* **2017**, *359*, 17.
[5] Y. Parvini, J. B. Siegel, A. G. Stefanopoulou, A. Vahidi, *IEEE Trans. Ind. Electron.* **2016**, *63*, 1574.
[6] K. V. G. Raghavendra, R. Vinoth, K. Zeb, C. V. V. Muralee Gopi, S. Sambasivam, M. R. Kummara, I. M. Obaidat, H. J. Kim, *J. Energy Storage* **2020**, *31*, 101652.
[7] P. Han, G. Xu, X. Han, J. Zhao, X. Zhou, G. Cui, *Adv. Mater.* **2018**, *8*, 1801243.
[8] J. Ding, W. Hu, E. Paek, D. Mitlin, *Chem. Rev.* **2018**, *118*, 6457.
[9] A. Jagadale, X. Zhou, R. Xiong, D. P. Dubal, J. Xu, S. Yang, *Energy Storage Mater.* **2019**, *19*, 314.
[10] G. Li, Z. Yang, Z. Yin, H. Guo, Z. Wang, G. Yan, Y. Liu, L. Li, J. Wang, *J. Mater. Chem. A* **2019**, *7*, 15541.
[11] R. Kang, W.-Q. Zhu, S. Li, B.-B. Zou, L.-L. Wang, G.-C. Li, X.-H. Liu, D. H. L. Ng, J.-X. Qiu, Y. Zhao, F. Qiao, J.-B. Lian, *Rare Met.* **2021**, *40*, 2424.
[12] S. Yi, L. Wang, X. Zhang, C. Li, W. Liu, K. Wang, X. Sun, Y. Xu, Z. Yang, Y. Cao, J. Sun, Y. Ma, *Sci. Bull.* **2021**, *66*, 914.
[13] X. Dai, S. Lei, J. Liu, Z. Shang, S. Zhong, X. Li, *J. Power Sources* **2021**, *498*, 229912.
[14] H. Liang, Z. Hu, Z. Zhao, D. Chen, H. Zhang, H. Wang, X. Wang, Q. Li, X. Guo, H. Li, *J. Energy Chem.* **2021**, *55*, 517.
[15] Y. Bai, Y. Hai, L. Cui, Y. Gong, *Energy Technol.* **2021**, *9*, 2000701.
[16] B. Akinwolemiwa, C. Wei, G. Z. Chen, *Electrochim. Acta* **2017**, *247*, 344.
[17] H. Wang, C. Zhu, D. Chao, Q. Yan, H. J. Fan, *Adv. Mater.* **2017**, *29*, 1702093.
[18] Y. Shao, M. F. El-Kady, J. Sun, Y. Li, Q. Zhang, M. Zhu, H. Wang, B. Dunn, R. B. Kaner, *Chem. Rev.* **2018**, *118*, 9233.
[19] G. G. Amatucci, F. Badway, A. Du Pasquier, T. Zheng, *J. Electrochem. Soc.* **2001**, *148*, A930.
[20] N. El Ghossein, A. Sari, P. Venet, in *VPPC*, Hangzhou, China, **2016**, p. 7791712.
[21] S. Zhang, *Battery Supercaps* **2020**, *3*, 1137.
[22] J. J. Lamb, O. S. Burheim, *Energies* **2021**, *14*, 979.
[23] H.-Y. Park, M.-S. Kim, T.-S. Bae, J. Yuan, J.-S. Yu, *Langmuir* **2016**, *32*, 4415.
[24] R. Black, S. H. Oh, J.-H. Lee, T. Yim, B. Adams, L. F. Nazar, *J. Am. Chem. Soc.* **2012**, *134*, 2902.
[25] Y. Kang, C. Deng, Y. Chen, X. Liu, Z. Liang, T. Li, Q. Hu, Y. Zhao, *Nanoscale Res. Lett.* **2020**, *15*, 112.
[26] B. Ludwig, Z. Zheng, W. Shou, Y. Wang, H. Pan, *Sci. Rep.* **2016**, *6*, 23150.
[27] D. Yang, A. Velamakanni, G. Bozoklu, S. Park, M. Stoller, R. D. Piner, S. Stankovich, I. Jung, D. A. Field, C. A. Ventrice, R. S. Ruoff, *Carbon* **2009**, *47*, 145.
[28] M. L. Divya, Y.-S. Lee, V. Aravindan, *Battery Supercaps* **2021**, *4*, 671.
[29] M. L. Divya, S. Jayaraman, Y.-S. Lee, V. Aravindan, *Chem. Eng. J.* **2021**, *426*, 130892.
[30] Š. Meškinis, A. Vasiliauskas, M. Andrulevičius, D. Peckus, S. Tamulevičius, K. Viskontas, *Mater.* **2020**, *13*, 1003.
[31] N. Elgrishi, K. J. Rountree, B. D. McCarthy, E. S. Rountree, T. T. Eisenhart, J. L. Dempsey, *J. Chem. Educ.* **2018**, *95*, 197.
[32] M. D. Levi, E. A. Levi, D. Aurbach, *J. Electroanal. Chem.* **1997**, *421*, 89.
[33] S. Zhang, M. Ding, K. Xu, J. Allen, R. Jow, *Electrochem. Solid-State Lett.* **2001**, *4*, A206.
[34] Z. Tai, Y. Liu, Q. Zhang, T. Zhou, Z. Guo, H. Liu, S. Dou, *Green Energy Environ.* **2017**, *2*, 278.
[35] K. Persson, V. A. Sethuraman, L. J. Hardwick, Y. Hinuma, Y. S. Meng, A. van der Ven, V. Srinivasan, R. Kostecki, G. Ceder, *J. Phys. Chem. Lett.* **2010**, *1*, 1176.
[36] P. Yu, B. N. Popov, J. A. Ritter, R. E. White, *J. Electrochem. Soc.* **1999**, *146*, 8.
[37] H. Gao, Q. Wu, Y. Hu, J. P. Zheng, K. Amine, Z. Chen, *J. Phys. Chem. Lett.* **2018**, *9*, 5100.
[38] B. P. Matadi, S. Geniès, A. Delaille, C. Chabrol, E. de Vito, M. Bardet, J.-F. Martin, L. Daniel, Y. Bultel, *J. Electrochem. Soc.* **2017**, *164*, A2374.